frontiers | Frontiers in Earth Science

TYPE Original Research
PUBLISHED 01 September 2022
DOI 10.3389/feart.2022.992900

OPEN ACCESS

EDITED BY
Simona Ferrando,
University of Turin, Italy

REVIEWED BY
Wang Fangyue,
Hefei University of Technology, China
Maryam Khosravi,
Isfahan University of Technology, Iran

*CORRESPONDENCE
Yirang Jang,
yirang@jnu.ac.kr
Sanghoon Kwon,
skwon@yonsei.ac.kr

SPECIALTY SECTION
This article was submitted to Petrology, a section of the journal Frontiers in Earth Science

RECEIVED 13 July 2022
ACCEPTED 09 August 2022
PUBLISHED 01 September 2022

CITATION
Samuel VO, Santosh M, Jang Y and Kwon S (2022), Role of acidic fluids in Earth's deep lithosphere: Insights from the Neoarchean magmatic roots of the Nilgiri Block, southern India. *Front. Earth Sci.* 10:992900. doi: 10.3389/feart.2022.992900

Role of acidic fluids in Earth's deep lithosphere: Insights from the Neoarchean magmatic roots of the Nilgiri Block, southern India

Vinod O. Samuel[1], M. Santosh[2,3], Yirang Jang[4]* and Sanghoon Kwon[1]*

[1]Department of Earth System Sciences, Yonsei University, Seoul, South Korea, [2]School of Earth Sciences and Resources, China University of Geosciences Beijing, Beijing, China, [3]Department of Earth Sciences, University of Adelaide, Adelaide, SA, Australia, [4]Department of Earth and Environmental Science, Chonnam National University, Gwangju, South Korea

Fluids play a major role in facilitating igneous/metamorphic processes in the Earth's crust and mantle. In this study, we investigate the nature and composition of fluids in Earth's interior by studying the lower crustal rocks. We compare accessory minerals (e.g., apatite, monazite, allanite, and titanite), their texture, mineral reactions and composition among regionally distributed metamorphosed mafic and felsic rocks representing the roots of Neoarchean arc magmatism from the Nilgiri Block of the Southern Granulite Terrane in India. Regional trends in accessory minerals show the formation of monazite, allanite, and titanite in the felsic rocks. Apatite is depleted in REEs in all the rock types, irrespective of the difference in their whole-rock chemistry. Textural features and mineral reactions show that these accessory minerals were affected by fluids present in the lower crustal conditions. By comparing our results with those from previous experimental results, we further show that acidic CO_2-H_2O-HCl-HF fluids stable in lower crustal conditions could have resulted in these chemical and textural features. Dielectric constant of water is high (10–35 compared to lower crustal conditions) in high-pressure and low-temperature conditions of subduction zones and the upper mantle. Such conditions would enhance dissociation of HCl (compared to lower crust) and result in acidic fluids during dehydration reactions in subduction zones and in the upper mantle. Our results have important implications in understanding the nature and composition of fluids in Earth's interior and would be helpful to model the tectonic and deep geochemical processes in both early and modern conditions in planetary interiors.

KEYWORDS

Neoarchean, lower-crust, accessory minerals, acidic fluids, subduction zone, upper mantle

Introduction

Magmatic and metamorphic processes release fluids (aqueous or supercritical) to deep lithosphere and mantle (Fyfe et al., 1978; Ague, 2014). Physical and chemical properties of fluids in the Earth's interior are key to model and interpret deep geochemical processes and element cycling. Water is predicted to be a major component in fluids in the Earth's crust and mantle (Thompson, 1992). Thermodynamic models indicate that low dielectric constant of water causes association of solutes (NaCl and HCl) in water at deep conditions (Eugster, 1986; Pan et al., 2013). The experimental and thermodynamic models of deep Earth processes suggest mixing of CO_2 and NaCl (more stable than components of HCl) in water, and could form immiscible H_2O-CO_2 and saline fluids (Manning, 2018). Recent molecular simulation studies on speciation in H_2O-CO_2 mixture at high temperature ($T > 200^{\circ}C$) high pressure ($P > 2$ GPa) conditions predict that H_2O-CO_2 mixing causes an increase in the concentration of carbonic acid (aqueous H_2CO_3) compared to aqueous CO_2 and suggest that fluid–rock interactions in Earth's subduction zones and upper mantle may occur in an acidic environment if proton hopping is possible (Pan and Galli, 2016; Stolte and Pan, 2019). Such fluids have important implications in mass transport and release of H_2O-CO_2 from subduction zones and upper mantle (Stolte and Pan, 2019; Castillo, 2022). It is challenging to test these results due to limitations in availability of natural fluid inclusions representing deep Earth, and also experimental, modelling, and spectroscopic methods to detect and interpret speciation in H_2O-CO_2-Cl system in high P-T conditions. Our approach to improve our knowledge is exploring factors controlling mineral reactions and partitioning of fluid components in natural minerals in the Earth's interior (Samuel et al., 2019; Kwon et al., 2020; Noh et al., 2020; Samuel et al., 2021).

In a previous study, we used the regional variations in high-halogen-bearing natural apatite grains to suggest presence of acidic fluids in the lower crust (750–900°C and 0.8–1 GPa) (Samuel et al., 2021). In this study, we provide further evidence of such conditions using accessory mineral reactions. We evaluate the role of fluids in lower crustal reactions of accessory minerals (i.e., apatite, monazite, titanite and allanite) using their composition, textural relationships and by comparing our results with previous experimental results. Our samples are from a tilted cross-section of arc magmatic root consisting of amphibolite, pyroxenite, metagabbro, and dioritic–tonalitic rocks in the southern part of Peninsular India (Samuel et al., 2014; Samuel et al., 2019). Based on our results we show that acidic CO_2-H_2O-HCl-HF fluids, in the absense of saline fluids or carbonic acid, could have facilitated solid state reactions of accessory minerals present in the lower crustal conditions. We further use this result to show the possible range of P-T conditions where such acidic fluids could be stable in Earth's lower crust, subduction zones, and upper mantle.

Geological setting

Dharwar Craton and lower crustal blocks

Southern part of the Peninsular India is composed of the Paleo- to Neoarchean Dharwar Craton in the north and the mosaic of Archean-Proterozoic lower crustal blocks accreted to it towards the south (Figure 1; Radhakrishna, 1989; Chadwick et al., 2000; Jayananda et al., 2018; Wang et al., 2020; Wang and Santosh, 2019; Mathew et al., 2022). These lower crustal blocks include the Mesoarchean Coorg Block, and the Neoarchean Nilgiri (NIL)-Biligirirangan (BR)-Shevaroy (SH)-Namakkal (NM)-Madras (MD) Blocks (Peucat et al., 2013; Santosh et al., 2013; Samuel et al., 2014; Santosh et al., 2015; George et al., 2019; Ratheesh-Kumar et al., 2020; Santosh, 2020; Yang et al., 2021; Anoop et al., 2022) adjacent to the Dharwar Craton. The crust-scale Palghat-Cauvery Suture/Shear System (PCSS) separates the Mesoarchean to Neoarchean blocks adjacent to the Dharwar Craton in the north from younger blocks in the south (Chetty et al., 2003; Santosh et al., 2009; Santosh et al., 2017; Gao et al., 2021; Yang et al., 2022; Yu et al., 2022). Major rock types in Mesoarchean to Neoarchean blocks to the south of the Dharwar Craton and north of the PCSS (Figure 1) mostly have metasediments, banded iron formation, pyroxenite, gabbroic, and tonalitic to granodioritic composition and undergone granulite to amphibolite facies metamorphism 2500–2450 Ma ago (Peucat et al., 2013; Santosh et al., 2013; Samuel et al., 2014; George et al., 2019; Ratheesh-Kumar et al., 2020; Santosh, 2020; Yang et al., 2021).

Nilgiri Block

For this study we use mafic and felsic samples from the lower crustal sections of Nilgiri Block, representing a triangular prism of crust uplifted up to ~2500 m above sea level (highlands) in the eastern side and ~900 m above sea level (lowlands) in the western part and along the shear zones (Figure 2). This block is bounded by two major crustal scale shear zones: the Moyar shear zone to the north and the Bhavani shear zone to the south (Bhaskar Rao et al., 1996; Raith et al., 1999; Meissner et al., 2002). Both shear zones converge at the eastern tip of the Nilgiri Block, and extend to the east as the Salem-Attur shear zone.

The Nilgiri highlands are characterized by metasediments, banded iron formation, amphibolite, pyroxenite, metagabbro in the north, two-pyroxene granulite in the transition zone, charnockite in the central and southern parts (Samuel et al., 2014; Samuel et al., 2015; Samuel et al., 2016; Samuel et al., 2018). The lowlands in the western part, and in the shear zones present towards the south and north of highlands consist of hornblende-biotite gneiss (Figure 2) (Samuel et al., 2014). All these rock types consist of rounded to sub-rounded minerals, and show additional textural indication (see below) of high-grade metamorphism.

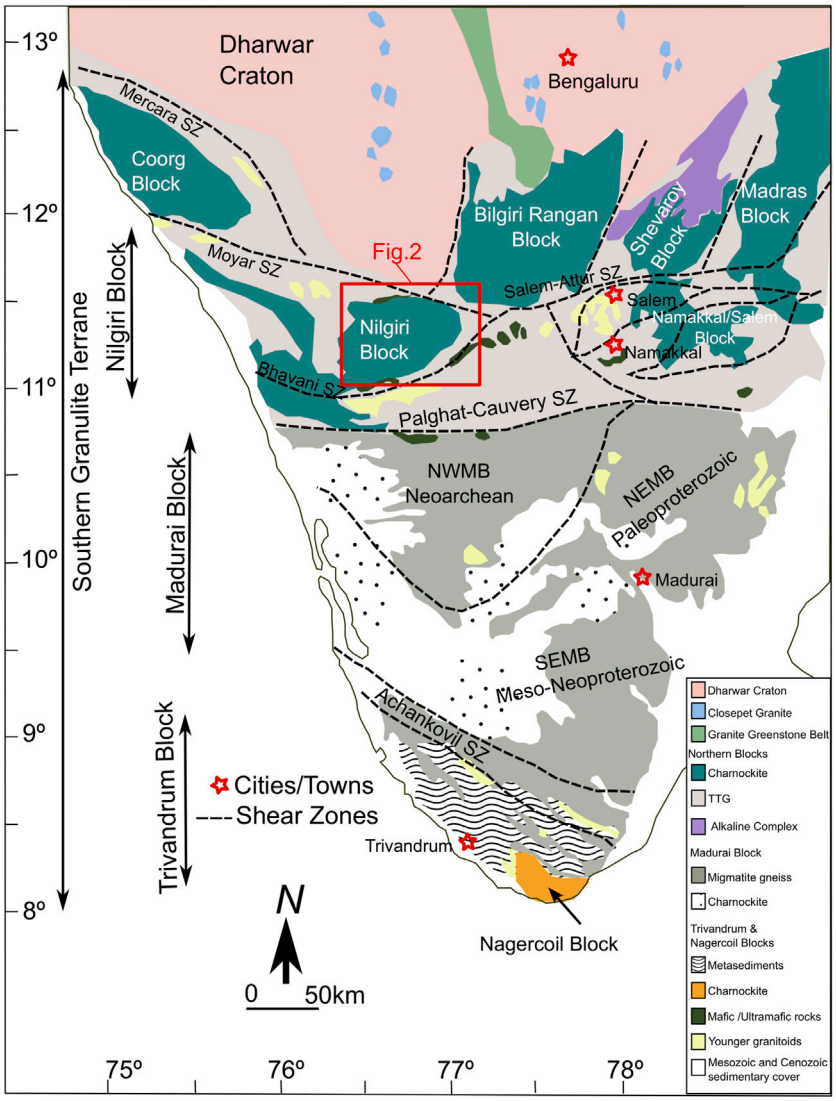

FIGURE 1
Regional geology and tectonic framework of southern India (modified after Samuel et al., 2018). The red box outlines the study area in the Nilgiri Block.

Metagabbro consists of garnet and clinopyroxene porphyroblasts with inclusions of orthopyroxene, amphibole and plagioclase, indicating high-pressure granulite facies metamorphism (Samuel et al., 2015). Two-pyroxene granulite and charnockite samples show dehydration textures like formation of anhydrous minerals (pyroxene) around hydrous minerals (biotite and amphibole) (Samuel et al., 2019). Thermo-barometric results indicate a regional trend in both temperature (−650–800°C) and pressure (~700–1100 MPa) from SW to NE across the Nilgiri highlands (Samuel et al., 2015; Samuel et al., 2018; Samuel et al., 2019). Abundant anti-perthite formation in these felsic samples along with K-feldspar veins forming around quartz, pyroxene and biotite etc., possibly indicate metasomatic alteration during/following peak metamorphism (Samuel et al., 2019). Further trends of regional oxide-sulfide mineralogy show that charnockite is abundant in rutile-ilmenite-pyrrhotite-chalcopyrite, whereas hemo- Ilmenite-magnetite-pyrite +/− (minor pyrrhotite-chalcopyrite) dominates in the two-pyroxene granulites and metagabbros (Samuel et al., 2019). These trends suggest a regional oxidation, where mafic granulite/metagabbro and two-pyroxene granulite samples are highly oxidized compared to the charnockites (Samuel et al., 2019). These results suggest interaction of oxidizing fluids during high-grade metamorphism (Samuel et al., 2019).

In addition, a recent study on the halogen content in apatite from major rock types in this block shows that metagabbro, two-

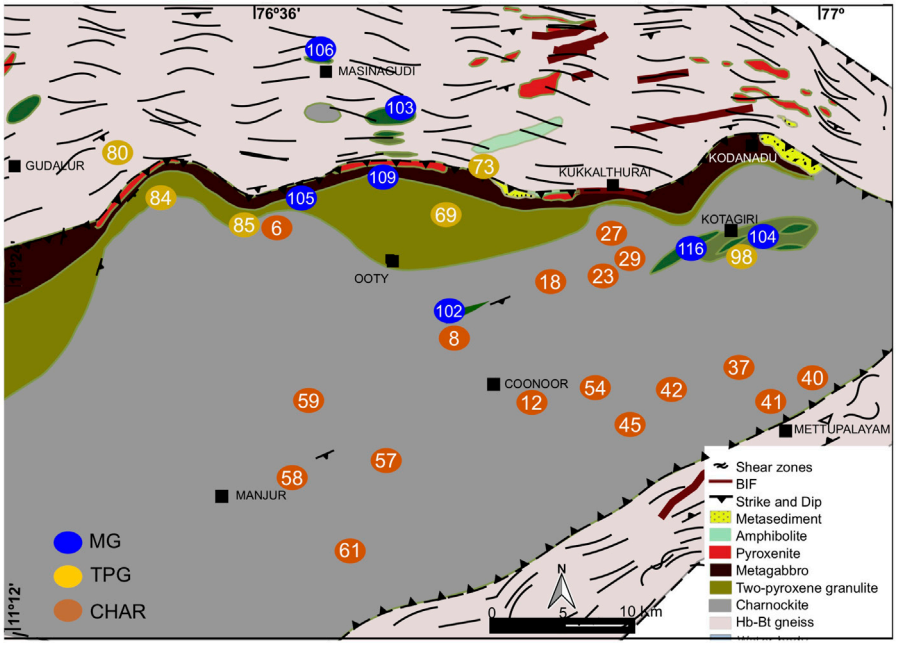

FIGURE 2
Geological map of the Nilgiri massif (modified after Samuel et al., 2021). Sample locations annotated by sample numbers are plotted on the map. The numbers are the same as those used in Samuel et al. (2021), and are also listed in the Supplementary Table S1. CHAR- charnockite samples, TPG- two-pyroxene granulite samples, and MG- metagabbro samples. This figure is created using QGIS 2.6.1 (https://www.qgis.org/en/site/) and modified using Inkscape version 0.92.2 (https://inkscape.org).

pyroxene granulite and few charnockite formed at higher *P-T* conditions have high Cl content (0.5–2.95 wt%). The observed Cl content in the apatite shows a decreasing trend with respect to the decrease in metamorphic grade (Samuel et al., 2021). Conversely, F content in the apatite is low in metagabbro compared to constant value of ~3 wt% in two-pyroxene granulite, charnockite and Hb-Bt gneiss. The results suggest the presence of acidic CO_2-H_2O-Cl-F fluid to incorporate high Cl composition in apatite at granulite facies condition (Brenan, 1993; Samuel et al., 2021). To further understand the role of fluids in deep processes, in this study, we investigate mineralogical, textural and rare earth elements compositional trends in apatite, monazite, allanite and titanite from the metagabbro/mafic granulite (MG), two-pyroxene granulite (TPG), charnockite (Char) and hornblende-biotite gneiss (HBG) samples.

Analytical techniques

Due to their small grain size, compositions of apatite, monazite, allanite and titanite were analyzed using JEOL JXA-8100 Superprobe, Electron Probe Micro Analyzer (EPMA), attached with 5 spectrometers housed at the Department of Earth System Sciences, Yonsei University, Seoul, South Korea. All the analysis was conducted using an accelerating voltage of 20 kV and beam current of 15 nA for apatite, allanite, titanite and 50 nA for monazite. An electron beam spot size of 15 μm for apatite and titanite, 1 μm for monazite and allanite were used. X-rays of F, Cl, Ca, Na, Al, Si, P, Mn and Fe were counted for 10 s at peak position and 5 s at background position. X-rays of REE's were counted for 50 s at peak position and 20 s at background position. F and Cl were measured first due to their volatile nature. To minimize the F X-ray excitation with time, elongated apatite grains were chosen for analysis based on the assumption that grains are oriented parallel to [0001]. Natural and synthetic silicates and oxides supplied by JEOL and ASTIMEX Standards Ltd., Canada, were used for calibration of Na, Al, Si, Mn, and Fe. F, Cl, Ca, P, and REE's were calibrated using the standards (F-apatite, Cl-apatite, and REE-Y-PO_4) provided by Prof. Daniel E. Harlov, GFZ Potsdam, Germany. Interference correction for REE's were performed using the database in (Pyle et al., 2002). Relative errors in EPMA are estimated to be <1%at the >10 wt% level, 5–10% at the 1–10 wt% level, 10–20% at the 0.2 to 1 wt% level, and 20–40% at the <0.1 wt% level. The data were reduced using the ZAF correction procedures supplied by JEOL. An average of between 5 and 35 grains of apatite, and their monazite grains (if present) were analyzed in each sample. The composition of all the observed allanite veins are measured. Titanite is observed and measured only in HBG samples. Concentration below detection limits (~500 ppm for Y + REE

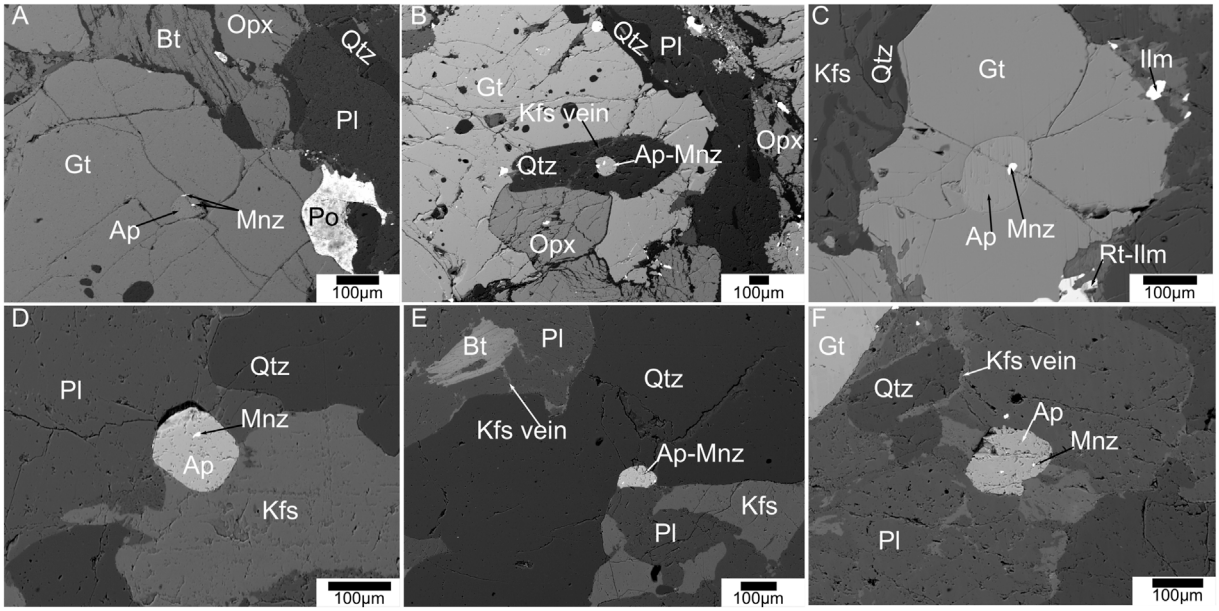

FIGURE 3
Back scattered electron images of equilibrium mineral assemblages and their textures in charnockite samples. Apatite grains with monazite blebs **(A)** within garnet; **(B)** near K-feldspar vein passing through quartz grains; **(C)** within garnet; **(D–F)** near K-feldspar veins in matrix of plagioclase and quartz.

and ~100 ppm for major elements) were discarded. During apatite recalculation procedure, H_2O (wt%) is added to make OH+F+Cl = 2 in the recalculated apatite mineral formula (Supplementary Table S2). Mole fractions of OH in apatite are calculated assuming the halogen site is filled with F, Cl, and OH ($X_{OH}Ap = 1\text{-}X_FAp\text{-}X_{Cl}Ap$).

Results

The locations of samples analyzed in this study and their petrography are given in Supplementary Table S1.

Petrography

Apatite is abundant in all the four rock types. Petrographical results show that apatite mostly crystallized as euhedral to subhedral grains and the grains are ~100 μm long and ~50 μm wide in size. They mostly occur in association with other major minerals along their grain boundaries as inclusions and along healed fractures (Figure 3). In the two-pyroxene granulite, apatite mostly occurs near K-feldspar veins and magnetite veins and pyroxene grain boundaries with magnetite rim (Figure 4). In metagabbro samples, a large proportion of apatite crystallization occurred along with magnetite veins and pyroxene grain boundaries with magnetite rim (Figure 5). In the HBG samples, apatite occurs mostly associated with amphibole grain boundaries (Figure 6C). The apatite grains show no compositional zoning in any of the samples. In metagabbro samples apatite grains are clean without any inclusions or compositional variation, while monazite is absent and rarely present in one sample (sample # 30-11) (Figure 5). In most cases, magnetite occurs as veins or chain of several grains along apatite grain boundaries in the metagabbro and two-pyroxene granulite samples (Figure 5). The two-pyroxene granulite and charnockite samples show abundant monazite inclusions and monazite grains along grain boundaries (Figures 3, 4). In few charnockites, two-pyroxene granulite and hornblende-biotite gneiss samples, allanite forms on the apatite grain boundaries (Figure 6). There is no monazite associated with apatite in hornblende-biotite gneiss samples (Figure 6C).

Metagabbro samples are generally devoid of monazite (Figure 5). Rarely one sample (sample # 30-11) shows few apatite grains with monazite. In two-pyroxene granulite and charnockite samples, however monazite is abundant and occurs as inclusions or along grain boundary of apatite grains (Figures 3, 4). Most monazite is present as multiple grains, as inclusion or along apatite grain boundaries with a round shape and a diameter of ~10 μm or less. In few samples, monazite grains occur minute oval shaped grains along long axis parallel to the C-axis of apatite with ~1 μm size or sometimes even smaller. Monazite is not observed in any other textural association in both charnockite and two pyroxene granulite. There are no

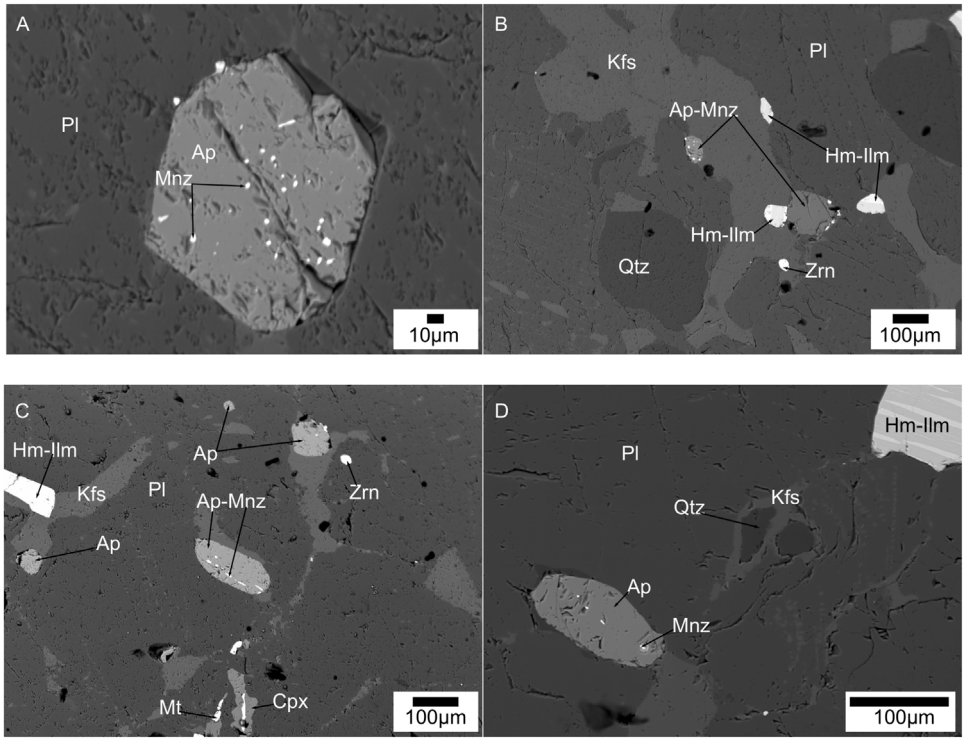

FIGURE 4
Back scattered electron images of mineral assemblages in equilibrium and their textures in two-pyroxene granulite samples. Apatite grains with monazite blebs **(A)** within plagioclase; **(B–D)** near K-feldspar veins in matrix of plagioclase and quartz.

independent monazite grains present in matrix of these samples. Monazite is absent in the hornblende-biotite gneiss samples (Figure 6).

Allanite is rarely present as veins at grain boundaries of apatite grains and found in three charnockite, one two-pyroxene granulite and two Hb-Bt gneiss sample (Figure 6). The allanite veins have a width of ~1 μm or less. There is no discrete allanite grains are observed in any samples. Titanites are present only in the hornblende-biotite gneiss samples (Figure 7). They appear in typical wedge-shaped crystals with a size range of ~2–0.5 mm. They occur as inclusions in amphibole and biotite grains, along grain boundaries, and also as discrete grains in the quartz feldspar matrix. Few titanite grains preserve hemo-ilmenite, and zircon inclusions in them (Figure 7B).

Mineral chemistry

The main constituents of apatite in all samples are Ca, P, OH, F, Cl and Fe (Supplementary Table S2). Apatite grains in all samples are heavily depleted in their Y + REE content (below 5000 ppm). This is common in all textural associations including inclusions in other minerals. Y + LREEs contribute to the observed REE content, and HREE content are below detection limit. LREEs such as La, Ce, Pr, Nd constitute the main REE contributor in most samples, whereas Y, Gd, and Dy are rarely present. In the metagabbro, two pyroxene granulite and few charnockite samples, apatite is relatively enriched in Cl up to 2.95–0.5 wt% compared to other charnockite and hornblende-biotite samples (Samuel et al., 2021). Fluorine component in the apatite grains is relatively low in metagabbro samples, however, and shows a constant composition of ~3 wt% in two pyroxene granulite, charnockite and hornblende-biotite sample (Samuel et al., 2021). Another important oxide in apatite is FeO, and its content is high (0.1–2.1 wt%) in all samples.

The major composition of the monazite is represented by LREEs such as La, Ce, Pr, Nd, Sm and Gd (Supplementary Table S3). Compositionally, these monazites are Th depleted, and its content is less than 0.05 wt%. Y is below detectable limits. The composition of LREEs in monazite in charnockite and two-pyroxene granulite samples shows similar trends. Monazite in these samples have La 5–16 wt%; Ce 26–35 wt%; Pr 2–5 wt%; Nd 11–22 wt%; Sm 0.6–5 wt%; Gd 0–2 wt%.

Similar to apatite and monazite, allanite is also enriched in FeO (8–12 wt%) and LREEs (Supplementary Table S4). The LREE content is substantially less in allanite compared to

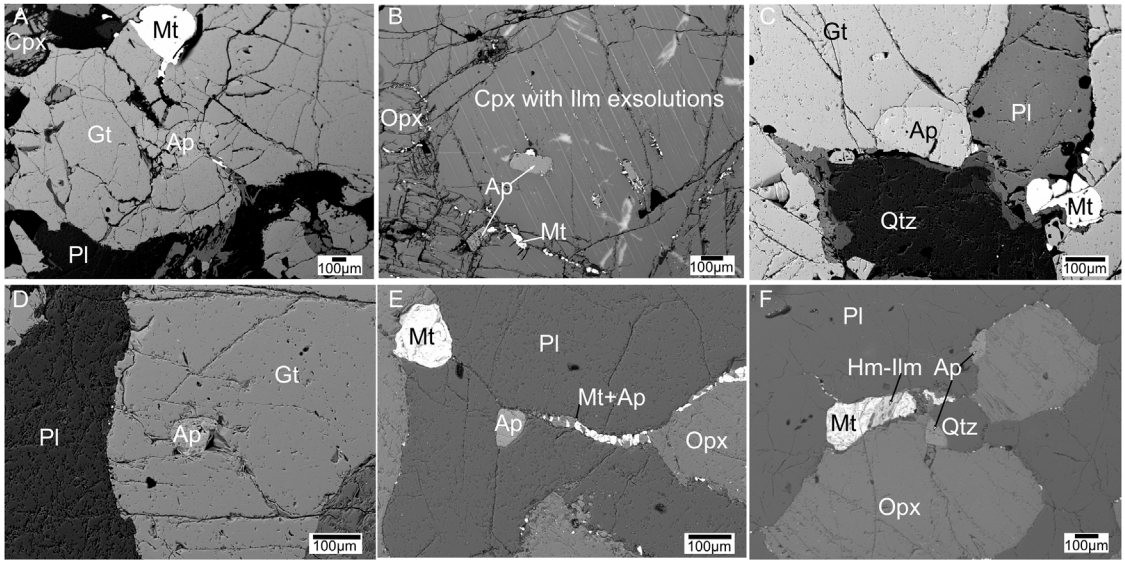

FIGURE 5
Back scattered electron images of mineral assemblages in equilibrium and their textures in metagabbro samples. Apatite grains (with no monazite blebs) **(A,D)** within garnet; **(B)** within clinopyroxene; **(C)** on garnet, plagioclase, quartz grain boundary; **(E)** along a magnetite-apatite vein passing through plagioclase; **(F)** on the orthopyroxene grain boundary.

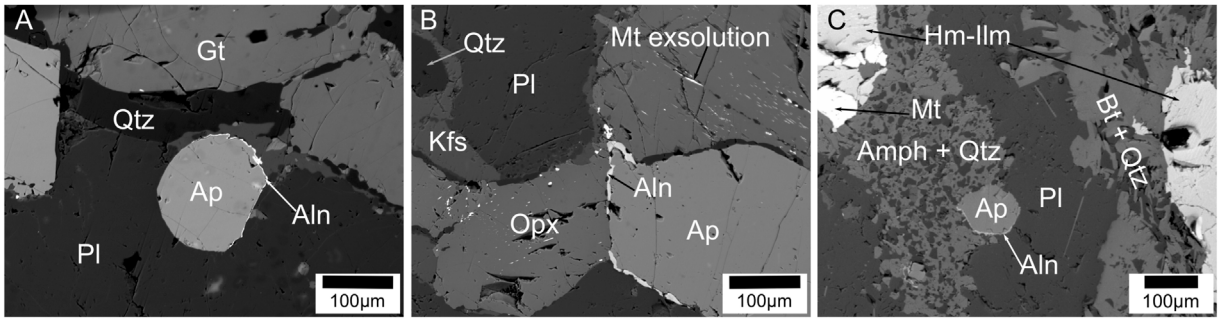

FIGURE 6
Back scattered electron images of allanite at apatite grain boundary. **(A)** allanite forming on apatite associated to plagioclase in charnockite sample; **(B)** allanite forming on apatite associated to orthorpyroxene in two-pyroxene granulite sample; **(C)** allanite forming on apatite associated to amphiboles in Hb-Bt gneiss sample.

monazite. LREE composition of allanite consists of La 1–5 wt %; Ce 3-10 wt%; Pr 0.5–1.5 wt%; Nd 0–4 wt%; Sm 0–0.3 wt%; Gd 0–0.5 wt%. Th and Y are below detection limits in all the samples.

Titanites contain trace amount of FeO (1–2 wt%) and Al_2O_3 (0.5–4 wt%) in addition to SiO_2, CaO and TiO_2 (Supplementary Table S5). Na_2O content is negligible. Th and Y are below detection limits. LREE composition of titanites consist of La 0–0.14 wt%; Ce 0-0.27 wt%; Pr 0–0.43 wt%; Nd 0–0.6 wt%; Sm 0–0.1 wt%; Gd 0–0.2 wt%.

Pseudosection modelling

To estimate the concentration of CO_2 in H_2O-CO_2 solutions present in the lower crustal conditions, we have modelled T—X_{CO2} pseudosections for mafic and felsic granulite samples from the Nilgiri Block. We have used mineral compositions of garnet, orthopyroxene and clinopyroxene and whole-rock chemistry data from Samuel et al. (2014).

Pseudosections were modelled with X_{CO2} on the X axis (0–1) and temperature on the Y axis (750–950°C). We have used the

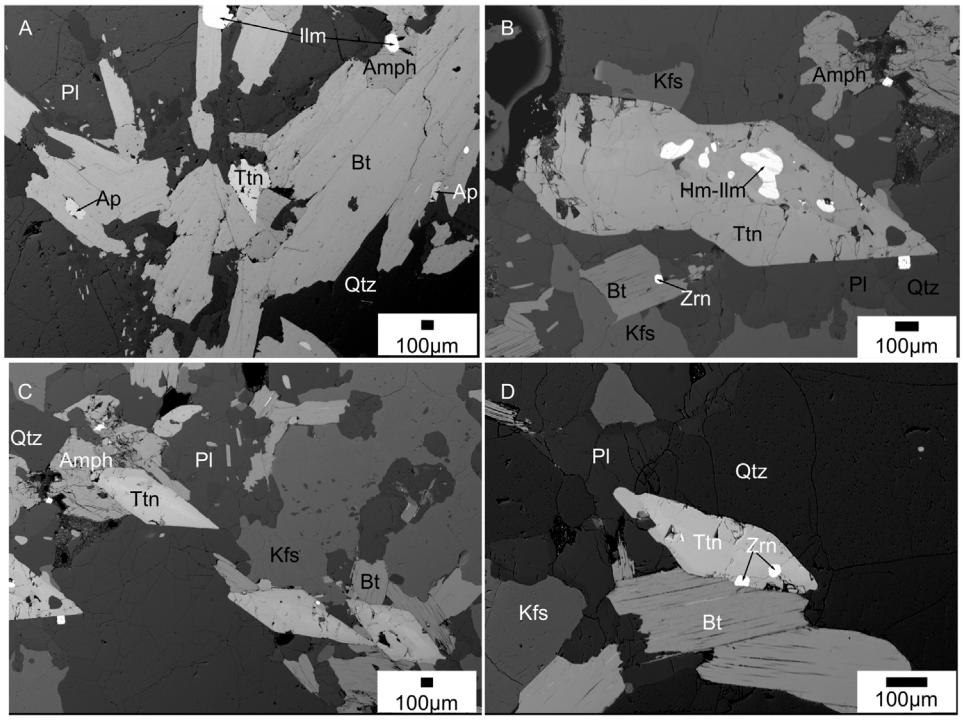

FIGURE 7
Back scattered electron images of titanite (sphene) formation in Hb-Bt gneiss samples. **(A)** Titanite and apatite associated to biotite laths; **(B)** Hemo-ilmenite inclusions in titanite associated to plagioclase-K-feldspar-quartz-biotite-amphibole matrix; **(C)** titanite grains associated to plagioclase-K-feldspar-quartz-biotite-amphibole matrix; **(D)** Titanite with zircon inclusions in a quartz-biotite-plagioclase-K-feldspar matrix.

Holland and Powell (2011) database (hp11ver.dat) implemented in the Perple_X (version 6.7.9) software of Connolly (2005) and H_2O-CO_2 fluid model of Holland and Powell (1991), Holland and Powell (1998). Following mineral solution models were used for modeling: clinopyroxene (Green et al., 2016); garnet (White et al., 2014); orthopyroxene (White et al., 2014); plagioclase and orthoclase (Holland and Powell, 2003); biotite (White et al., 2014); amphibole (Green et al., 2016); and magnetite (White et al., 2002). The solution model for partial melts was taken from Green et al. (2016). The solid solution model for ilmenite coexisting with magnetite was used for ilmenite (Andersen and Lindsley, 1988). The O_2 value was estimated using the equation $2FeO + O = Fe_2O_3$, with the fraction of Fe^{3+} set equal to 0.12 for mafic and felsic rock types (Rebay et al., 2010; Palin et al., 2016). The whole-rock chemistry of two samples (mole percent) used for modeling are given below:

Mafic granulite: SiO_2=50.33; TiO_2=0.77; Al_2O_3=8.18; FeO=11.50; MgO=13.92; CaO=12.95; Na_2O=1.94; O_2=0.345.

Felsic granulite: SiO_2=66.99; TiO_2=0.54; Al_2O_3=10.01; FeO=5.88; MgO=4.94; CaO=6.43; K_2O=0.75; Na_2O=4.17; O_2=0.177.

Our results (Figure 8) suggest that orthopyroxene (X_{Mg} = 0.49–0.65) is stable in the felsic granulites at X_{CO2} = 0.4 and above (below 900°C). Previous geothermobarometry results suggest that mineral reactions in felsic granulites might have occurred ~750–800°C (Samuel et al., 2019). Above 900°C, mineral assemblages in the sample are mostly stable at lower X_{CO2} conditions. In the case of mafic granulite sample (orthopyroxene X_{Mg} = 0.5–0.68), at higher P-T conditions of 850–900°C and X_{CO2} = 0.5 and above, representative mineral assemblages are stable. Even up to 950°C, orthopyroxene in not stable at or below X_{CO2} of 0.5 in the mafic samples. Comparison of P-T estimates using exchange thermobarometers (750–900°C; Samuel et al., 2015; Samuel et al., 2019), and X_{CO2} estimation in this study shows that relatively high concentration of X_{CO2} conditions existed during the lower crustal processes generated observed mineral assemblages in these samples.

Discussion

Textural features of metasomatism during metamorphism

Petrographic studies of the rocks from Nilgiri Block show that apatite with monazite blebs occur mostly in the felsic rock types (i.e., charnockite and two pyroxene granulite) (Figures 3, 4). Previous experimental and transmission electron microscopic

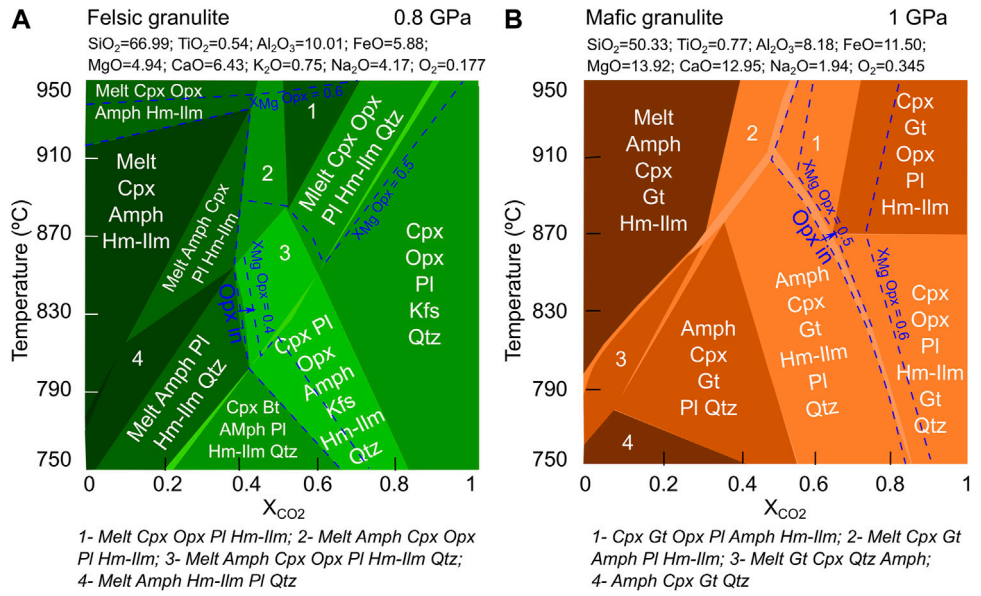

FIGURE 8
X_{CO2}-Temperature pseudosections modelled using compositions of felsic and mafic samples. **(A)** Pseudosection of felsic sample at 0.8 GPa. Blue dashed line represents orthopyroxene (X_{Mg}) composition. **(B)** Pseudosection of mafic sample at 0.8 GPa. Blue dashed line represents orthopyroxene (X_{Mg}) composition. Both pseudosections show that main mineral assemblage in both samples are stable at relatively high CO_2 concentration (X_{CO2} > 0.5).

(TEM) investigations on growth/precipitation of monazite blebs on apatite at granulite facies conditions show that the reacted region is characterized by numerous nano-channels through which fluids interacted with apatite to form monazite (Harlov et al., 2005). The presence of allanite veins around apatite grain boundaries also indicate their precipitation by fluids passing along grain boundaries and fractures (Figure 6). Titanite grains in Hb-Bt gneiss have hemo-ilmenite inclusions, possibly indicating that Ti is removed from ilmenite to form titanite by enriching hematite component in ilmenite by fluids (Figure 7) (Harlov and Hansen, 2005). Presence of such textural features in all the samples collected regionally show that these rocks were significantly altered by fluids during regional scale metamorphism after their igneous crystallization.

Rare earth elements composition of accessory minerals

Accessory minerals such as apatite, zircon, monazite, allanite and titanite in metamorphosed magmatic rocks show important REE distribution patterns useful for understanding their petrogenesis. In this study, apatite grains in both felsic and mafic rocks are depleted in REEs. Monazite blebs in charnockite and two-pyroxene granulite are enriched in LREEs (Figures 9A,B). Zircon grains in all these rock types of this terrane are enriched in HREEs in their core and rim, and are depleted in LREEs (Samuel et al., 2014). REEs significantly partition to apatite during the crystallization of felsic rocks (Prowatke and Klemme, 2006). Whole-rock HREE content does not show any variation among different rock types in this block (Figures 9C–F; Supplementary Table S6). However, whole rock LREE content shows variation between felsic (i.e., two-pyroxene granulite, charnockite and Hb-Bt gneiss; Figures 9C–E; Supplementary Table S6) and mafic (i.e., metagabbro: Figure 9F; Supplementary Table S6) rock types. LREEs are depleted in mafic rocks compared to felsic rocks (Figures 9C–F; Supplementary Table S6). Among felsic rocks two-pyroxene granulite shows the maximum LREE enrichment compared to charnockite and Hb-Bt gneiss.

In general, igneous apatite crystallized from granodioritic magma (of charnockite, two-pyroxene granulite, and Hb-Bt gneiss) would have partitioned high amount of REE to apatite (Prowatke and Klemme, 2006). This indicates that REEs were effectively removed from apatite during high-grade metasomatic process at least in case of felsic rocks. New monazite grains present along with apatite in the charnockite and two-pyroxene granulite samples (Figures 3, 4). These monazites are markedly enriched in LREEs and depleted in Th and U (Figures 9A,B). All rock types (felsic and mafic) show depletion in Th and U in their whole-rock chemistry, possibly indicating nature of their protolith (Samuel et al., 2014). Formation of LREE enriched monazite blebs on apatite suggest interaction of fluids

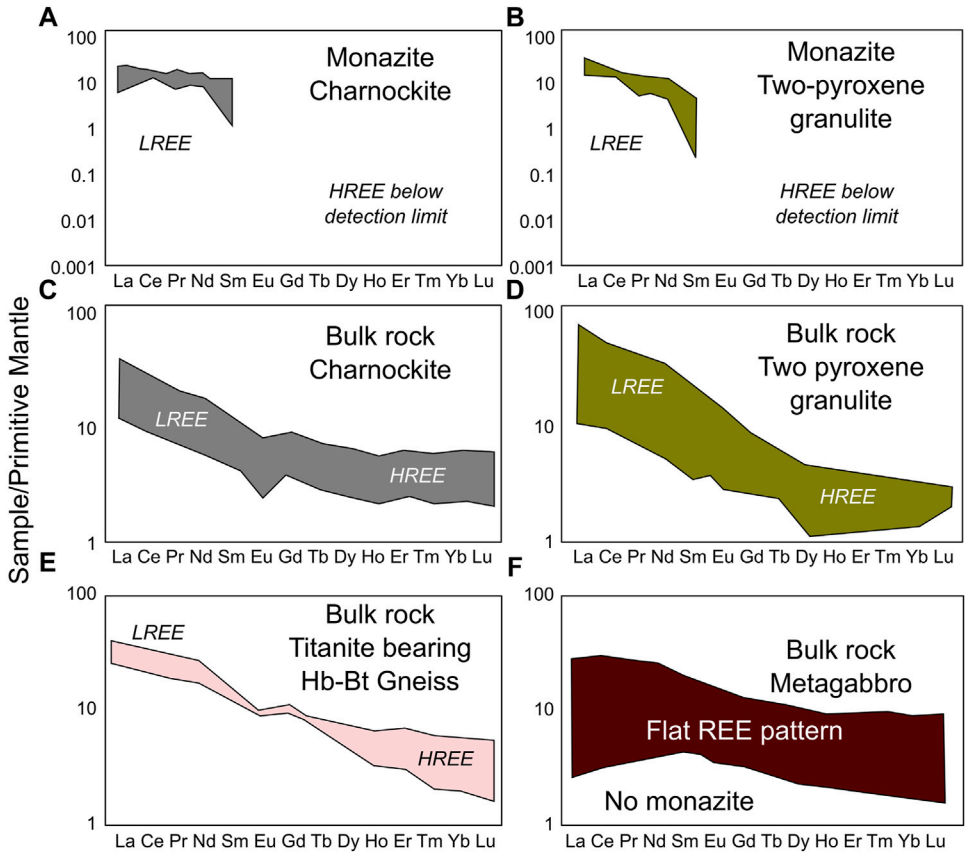

FIGURE 9
Primitive mantle-normalized REE patterns for samples from Nilgiri Block. Primitive mantle values from McDonough et al. (1991). **(A)** REE pattern of monazite blebs present on apatite grains present in charnockite samples. **(B)** REE pattern of monazite blebs present on apatite grains present in two-pyroxene granulite samples. **(C–F)** Since apatite REE composition depend on whole-rock REE, we compare apatite REE patterns with whole-rock REE patterns for different rock types from Nilgiri Block [data taken from Samuel et al. (2014) and Raith et al. (1999); Supplementary Table S6].

(Harlov et al., 2005). Therefore, it would be reasonable to correlate formation of LREE enriched monazite grains and allanite veins on grain boundaries of apatite grains with loss of LREE from original apatite (LREE enriched) grains in the felsic granulites. In the Hb-Bt gneiss samples, apatite grains are depleted in REEs, Th, and U similar to other rock types. Mostly allanite and titanite control the LREE budget in the Hb-Bt gneiss samples. The absence of formation of monazite blebs on apatite in the mafic rocks is most probably due to low LREE's, Th, U in protolith of mafic rocks and in apatite.

Role of acidic fluids during metamorphism

Previous studies in Nilgiri Block using fluid inclusions, mineralogical, textural, compositional, isotopic and thermodynamic data suggest that H_2O-CO_2 or H_2O-CO_2-NaCl (brines/saline fluids) or CO_2-H_2O-HCl-HF fluids were involved during high-grade metamorphism (Santosh, 1986; Touret and Hansteen, 1988; Santosh, 1992; Srikantappa et al., 1992; Dunai and Touret, 1993; Samuel et al., 2019; Samuel et al., 2021). On the other hand, aqueous NaCl is not considered as an effective agent in incorporating high Cl content in apatite, and also removing Y + REEs from them, if they are charge balanced by Na (Brenan, 1993; Hansen and Harlov, 2007; Samuel et al., 2021). The aqueous NaCl fluid is incapable of removal of Na^+ from apatite structure to destabilize $(Y + REEs)^{3+}$ and Ca^{2+} charge balance exists through the following coupled substitutions (Pan and Fleet, 2002; Hansen and Harlov, 2007)

$$Na^+ + (Y + REE)^{3+} \leftrightarrow 2Ca^{2+} \quad (1)$$

REE's could also be stabilized by coupled substation with Si in the original apatite grain. The reaction of britholite ($Ca_2REE_3Si_3O_{12}F$) can be shown as below (Hansen and Harlov, 2007).

$$Ca_2REE_3Si_3O_{12}OH + Ca_5P_3O_{12}OH + 14H^+ = 3\,(REE)PO_4 + 3SiO_2 + 7Ca^{2+}\,(\text{in fluid}) + 8H_2O \quad (2)$$

However, no additional quartz formation is observed anywhere near the monazite blebs. Therefore, it is reasonable to consider that REE's are stabilized through coupled substitution with Na. Also, we have observed that, as the britholite component increases in the apatite, allanite forms along grain boundaries of apatite grains in the metagabbro, charnockites, two-pyroxene granulites and Hb-Bt gneiss samples. We could consider that allanite formation could be preferred over monazite, if britholite component is abundant in apatite. Such allanite forming reactions could be represented as below.

$$Ca_2REE_3Si_3O_{12}OH + H\,(Cl, F) + 3Al = CaREEAl_3Si_3O_{12}\,(Cl, F) + H_2O + Ca^{2+} + 2REE \quad (3)$$

$$Ca_2REE_3Si_3O_{12}OH + 6.01 \times 10^{-17}P + H\,(Cl, F) + 3Al = 6.01 \times 10^{-17}\,(REE)PO_4 + Ca\,(REE)Al_3Si_3O_{12}\,(Cl, F) + H_2O + Ca^{2+} + 2REE \quad (4)$$

Thus, aqueous NaCl (at any pH) might retain REEs in apatite in contrast to REE and Na depleted nature of apatite grains in this terrane. Further, the high Cl (0.1–2.95 wt%) and F (0.78–3.5 wt %) contents in apatite [$Ca_{10}(PO_4)_6(F,Cl,OH)_2$] grains might indicate that the C-O-H-Cl-F fluid was highly acidic while interacting with these rocks (Samuel et al., 2021). Experimental results using 1 and 2 N HCl and H_2SO_4 solutions at temperatures of 300, 600, and 900°C and pressures of 500 and 1,000 MPa show that acidic fluids would generate the observed depletion in REEs in apatite and formation of monazite blebs (Harlov et al., 2005; Hansen and Harlov, 2007). The acidic nature of fluids (hydrochloric acid or carbonic acid) could make them a good agent of metamorphic recrystallization processes (either by diffusion or dissolution-reprecipitation).

The reaction of such apatite grains with acidic fluids (other than saline solutions) to form monazite could be represented by following equation,

$$[Ca_{5-2x}, Na_x, (Y + REE)_x]P_3O_{12}OH + x[2\,Ca^{2+} + P^{5+}] + H\,(Cl, F) = Ca_5P_3O_{12}\,(Cl, F) + x\,(Y + REE)PO_4 + x[Na^+] + H_2O \quad (5)$$

The mineral chemistry data of apatite grains in mafic and felsic rocks from the Nilgiri Block show that apatite grains are enriched in FeO or Fe_2O_3. Therefore, removal of (Y + REE) from the apatite structure might be charge balanced by incorporating Fe available in the fluids into apatite structure through following Eqs 6, 7.

$$Na^+ + (Y + REE)^{3+} \leftrightarrow 2Fe^{2+} \quad (6)$$

$$(Y + REE)^{3+} \leftrightarrow Fe^{3+} \quad (7)$$

The abundance of magnetite at apatite grain boundaries and as veins also supports such possibility of abundance of Fe in infiltrating acidic C-O-H-Cl-F fluid. This probably indicates the lattice contraction during dehydration (OH-Cl exchange) of apatite grains. This would cause the release of LREE's and led to the formation of monazite/allanite on them. Such acidic fluids could also have caused leaching of Ti from ilmenite to form titanite in the Hb-Bt gneiss samples. These features indicate that acidic C-O-H-Cl-F fluids were able to generate observed minerals, textures, LREE redistribution during lower crustal processes.

Nature and composition of fluids in the lower crust

Understanding the composition of acidic C-O-H-Cl-F fluid is important in gaining insights into the deep Earth processes. The presence of hydrous minerals, composition of fluid inclusions, and spectroscopic investigations of OH content in anhydrous minerals all indicate that H_2O is a major component of fluid in lithosphere and upper mantle conditions (Thompson, 1992). Previous fluid inclusion studies suggest that H_2O-CO_2 is a major component in lower crustal fluids (Santosh, 1986; Touret and Hansteen, 1988; Santosh et al., 1990; Srikantappa et al., 1992; Dunai and Touret, 1993). Results of pseudosection modelling in this study show that major mineral assemblages in the felsic and mafic samples require a relatively high concentration of CO_2 in the fluid (X_{CO2} = 0.5 or above; Figure 8). However, molecular dynamics simulations show no evidence for the formation of H_2CO_3 (aq) below 2.4 GPa, and suggest that below 2.4 GPa and 250°C (523 K) (at shallower conditions) CO_2 becomes a major component of fluids (Pan and Galli, 2016; Stolte and Pan, 2019). Therefore, H_2O and CO_2 are major components of these fluids in the lower crustal conditions.

In the interior of the Earth, dissolved NaCl (ion pairs, Na+, Cl-) components in H_2O are predicted to be more stable compared to components of HCl (Barnes et al., 2018). However, our previous results show that high Cl in the natural apatite grains could be incorporated by hydrochloric acid with modest Cl and F concentrations and suggest that saline fluids (at any pH) might not be a major component in fluids present in the lower crust (Samuel et al., 2021). At lower crustal conditions, where the dielectric constant of water is ~10 (Eugster, 1986; Pan et al., 2013), an acidic nature of reactions indicates that the dissociation constant ($K_{HCl/HF\text{-}H2O}$) is moderately high enough to dissolve Cl and F. Our results in this study further suggest that the formation of monazite blebs and allanite rims on apatite could have formed in acidic fluids (except saline fluids). In the absence of carbonic acid (H_2CO_3-H_2O) and saline fluids (NaCl-H_2O) we suggest that the composition of fluids in the lower crust are most probably be represented by a CO_2-H_2O-HCl-HF composition, where high HCl/HF fugacity could be correlated to their moderately high dissociation constant ($K_{HCl\text{-}H2O}$) and an acidic environment in the lower crust. These fluids could be internally generated (granulite facies dehydration during collision of continental blocks) or

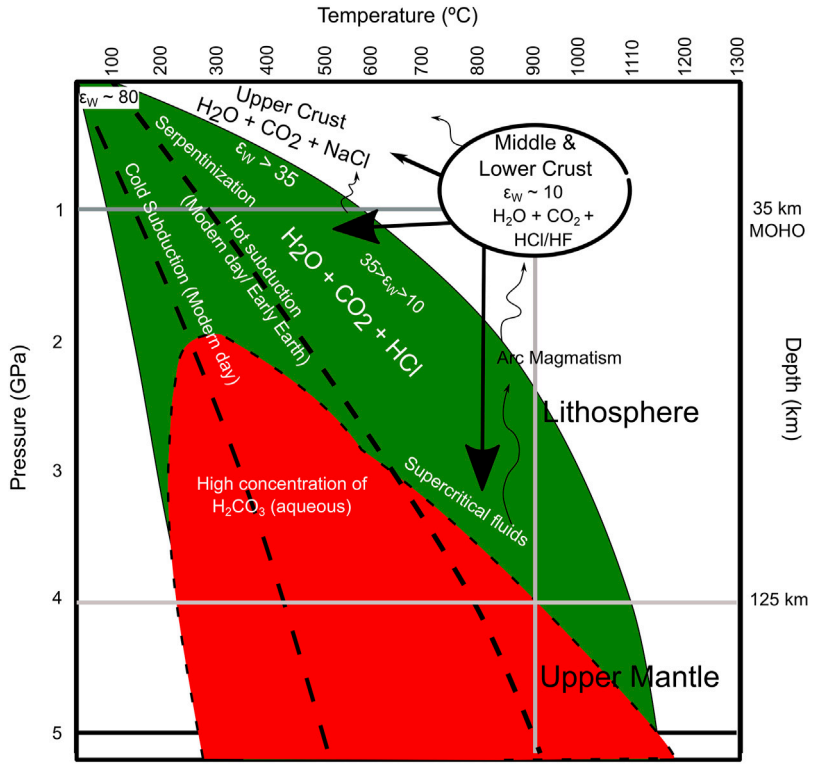

FIGURE 10
Schematic diagram representing P-T conditions of acidic CO_2-H_2O-HCl-HF fluids in lower crust, subduction zone, and upper mantle. Where ε_W is dielectric constant of water. Our results of acidic conditions at lower crust, where ε_W ~ 10 suggest that dissociation constant of solutes is moderately high in water ($K_{HCl/HF}$) at the lower crustal conditions. Therefore, below ~800°C and above 1GPa, acidic CO_2-H_2O-HCl-HF fluids could exist in most of the subduction zone (both cold and hot subduction existed throughout Earth's history and today (Thompson, 1992)) and upper mantle conditions. Concentration of carbonic acid (red area) increase above 2.4 GPa and 250°C in most of the upper mantle conditions (Pan and Galli, 2016; Stolte and Pan, 2019). Therefore, Earth's interior is mostly acidic in dehydration reactions (if minerals incorporate significant amount of Cl and CO_2) below Mohorovicic Discontinuity (MOHO).

externally derived (mafic underplating) or a mix of the two in a Cl rich environment. These aqueous acidic fluids might not dissolve other mineral forming components on a large-scale due to their low dielectric constant (low polarization) and low dissociation constant (low hydrogen bonding) at lower crustal conditions. The lattice contraction of apatite grains during dehydration (OH-Cl exchange) and fast diffusion (Bedford et al., 2017) of mineral-forming components (no dissolution-reprecipitation) facilitated by fluids might have caused the formation of monazite/allanite on apatite grains.

Implications

Stability of acidic HCl-HF in CO_2-H_2O fluids in the lower crust suggest that solutes will be comparatively more dissociated (higher $K_{HCl/HF\text{-}H2O}$) in dehydrating environments (with no external saline pore fluids) when the dielectric constant of water (ε_W) is 10–35 (Figure 10). These conditions of high ε_W at $p > 1$ GPa and T < 800°C are represented across larger sections of subduction zones and the upper mantle in different scenarios-such as cold and hot subductions in the modern and/or early periods on Earth as well as on other planets (Figure 10). Our results suggest that ε_W between 10 and 35 would cause a mild increase in the dissociation constants of NaCl and HCl ($K_{NaCl\text{-}H2O}$ and $K_{HCl\text{-}H2O}$). However, due to low or zero porosity (Chen et al., 2020) of subducting lithologies, saline pore fluid is most probably not being transported to greater depths (~ above 20–25 km). Therefore, saline pore fluids might not be present during the dehydration of the lower crust, subduction zones and the upper mantle. Saline pore fluids could be stable in the upper crust with high porosity, where ε_W > 35 (limit of NaCl dissolution in water). Our results suggest that in rock buffered environments, an increase in the K_{HCl} and ε_W (10–35) in deeper conditions (at T < 800°C) shows that we could expect acidic CO_2-H_2O-HCl-HF fluids during dehydration reactions (if minerals contain Cl) in the lower crust, subduction zones and the upper mantle. Further,

molecular dynamic simulations suggest that above 2.4 GPa and 250°C (523 K), carbonic acid concentration would increase in CO_2-H_2O fluids. Therefore, it is reasonable to consider that most of subduction and upper mantle geochemical processes below the Mohorovicic Discontinuity (MOHO) occur in an acidic environment. An increase in concentration of H_2CO_3 and HCl in fluids (aqueous or supercritical) in subduction zones and the upper mantle could also cause an increase in the dissolution of carbonate minerals in subducting slabs and release more CO_2 (than considered in existing models) to the mantle wedge and lower crust, and finally to the atmosphere causing global climatic variations. However, possibilities of diffusion or dissolution or dissolution-reprecipitation, and transport capacities of CO_2-H_2O-HCl-HF needs to be verified in future studies. Due to low dielectric constant and dissociation constant of aqueous acidic fluids, supercritical fluids might be the agent of large-scale mass transport in deeper conditions in Earth and other planets (e.g., Mars, Venus). However, the stability of supercritical fluids is highly dependent of variations in the geothermal gradient in planetary interiors through time.

Conclusion

1) Metagabbro in the Nilgiri Block of southern India is depleted in LREEs and contains high Cl-apatite grains depleted in REEs. No monazite blebs are associated with apatite grains.
2) Felsic rocks (charnockite, and two-pyroxene granulite) are enriched in LREEs. The REE-depleted apatite grains forms monazite blebs and/or allanite veins. Monazite and allanite are enriched in LREEs. In the Hb-Bt gneiss, apatite is depleted in REE's, allanite and titanite are enriched in LREEs. Lattice contraction of apatite grains during dehydration (OH-Cl exchange) and fast diffusion of mineral-forming components in fluids might have caused the formation of monazite/allanite on apatite.
3) Acidic CO_2-H_2O-HCl-HF fluids present during regional dehydration reactions during metamorphism might have acted as efficient agent for the diffusion of Fe, Ti, LREEs on a micro-meter scale. These internally or externally derived fluids (with low dissolved components) passed through the fractures and grain boundaries, and moved upwards through different rock types, facilitating solid state reactions.
4) The presence of acidic CO_2-H_2O-HCl-HF fluids, where water has a dielectric constant of ~10, implies high dissociation of solutes in subduction zones and the upper mantle (ε_W ~ 10–35). Therefore, geochemical processes below MOHO might occurs mainly in acidic conditions, if Cl, F and CO_2 (incorporated in minerals) are transported into the deep Earth.

Data availability statement

The original contributions presented in the study are included in the article/Supplementary Material, further inquiries can be directed to the corresponding authors.

Author contributions

VS, SK, and YJ. conceived the project. VS performed petrographic and EPMA analyses, and data evaluation. VS, SK, and MS. contributed to interpretation and the writing of an earlier draft. All authors equally contributed to interpretation and final manuscript writing.

Funding

This research was supported by 2017R1A6A1A07015374 (Multidisciplinary study for assessment of large earthquake potentials in the Korean Peninsula) through the National Research Foundation of Korea (NRF) funded by the Ministry of Science and ICT, Korea to VS, NRF-2019R1A2C1002211 to S.K., and NRF-2021R1C1C101057011 to YJ. Funding from the Ministry of Earth Sciences, Government of India projects MoES/ATMOS/PP-IX/09 and MoES/P.O. (Geosci)/26/2014 for field work and sample preparation while VS. was a PhD student at the Centre for Earth Sciences, Indian Institute of Science, Bangalore, India is also acknowledged.

Conflict of interest

The authors declare that the research was conducted in the absence of any commercial or financial relationships that could be construed as a potential conflict of interest.

Publisher's note

Supplementary material

The Supplementary Material for this article can be found online at: https://www.frontiersin.org/articles/10.3389/feart.2022.992900/full#supplementary-material

References

Ague, J. J. (2014). "Fluid flow in the deep crust," in *Treatise on geochemistry*. Editors H. D. Holland, and K. K. Turekian (Oxford: Elsevier), 13, 203–247. doi:10.1016/B0-08-043751-6/03023-1

Andersen, D. J., and Lindsley, D. (1988). Internally consistent solution models for Fe6Mg6Mn6Ti oxides: Part 1. *Amer. Min.* 73, 714–726.

Anoop, K. S., Anilkumar, Y., Santosh, M., Yu, B., Delna-Joy, K., Kavyanjali, K. V., et al. (2022). Magmatic and metamorphic evolution of a layered gabbro-anorthosite complex from the Coorg Block, southern India: Implications for Mesoarchean suprasubduction zone process. *Gondwana Res.* 103, 105–134. doi:10.1016/j.gr.2021.07.026

Barnes, J. D., Manning, C. E., Scambelluri, M., and Selverstone, J. (2018). in *The behavior of halogens during subduction-zone processes" in the role of halogens in terrestrial and extraterrestrial geochemical processes: Surface, crust, and mantle*. Editors D. E. Harlov and L. Aranovich (Berlin: Springer), 545–590.

Bedford, J., Fusseis, F., Leclère, H., Wheeler, J., and Faulkner, D. (2017). A 4D view on the evolution of metamorphic dehydration reactions. *Sci. Rep.* 7, 6881. doi:10.1038/s41598-017-07160-5

Bhaskar Rao, Y. J., Chetty, T. R. K., Janardhan, A. S., and Gopalan, K. (1996). Sm–Nd and Rb–Sr ages and PT history of the archean sittampundi and Bhavani layered meta-anorthosite complexes in cauvery shear zone, south India: evidence for neoproterozoic reworking of archean crust. *Contributions Mineralogy Petrology* 125, 237–250. doi:10.1007/s004100050219

Brenan, J. M. (1993). Partitioning of fluorine and chlorine between apatite and aqueous fluids at high pressure and temperature: Implications for the F and Cl content of high P-T fluids. *Earth Planet. Sci. Lett.* 117, 251–263. doi:10.1016/0012-821x(93)90131-r

Castillo, P. R. (2022). Arc magmatism and porphyry-type ore deposition are primarily controlled by chlorine from seawater. *Chem. Geol.* 589, 120683. doi:10.1016/j.chemgeo.2021.120683

Chadwick, B., Vasudev, V. N., and Hegde, G. V. (2000). The Dharwar craton, southern India, interpreted as the result of Late Archaean oblique convergence. *Precambrian Res.* 99, 91–111. doi:10.1016/S0301-9268(99)00055-8

Chen, J., Kuang, X., and Zheng, C. (2020). An empirical porosity-depth model for Earth's crust. *Hydrogeol. J.* 28, 2331–2339. doi:10.1007/s10040-020-02214-x

Chetty, T. R. K., Bhaskar-Rao, Y. J., and Narayana, B. L. (2003). "A structural cross section along krishnagiri–palani corridor, southern granulite terrain of India," in *Tectonics of southern granulite terrain*. Editor M. Ramakrishnan (India: Geological Society of India-Memoir), 50, 255–278.

Connolly, J. A. D. (2005). Computation of phase equilibria by linear programming: A tool for geodynamic modeling and its application to subduction zone decarbonation. *Earth Planet. Sci. Lett.* 236, 524–541. doi:10.1016/j.epsl.2005.04.033

Dunai, T. J., and Touret, J. L. R. (1993). A noble gas study of a granulite sample from the Nilgiri Hills, southern India: Implications for granulite formation. *Earth Planet. Sci. Lett.* 119, 271–281. doi:10.1016/0012-821X(93)90138-Y

Eugster, H. P. (1986). Minerals in hot water. *Amer. Min.* 71, 655–673.

Fyfe, W. S., Price, N., and Thompson, A. B. (1978). *Fluids in the Earth's crust*. Netherlands: Elsevier.

Gao, P., Santosh, M., Yang, C. X., Kwon, S., and Ramkumar, M. U. (2021). High Ba–Sr adakitic charnockite suite from the nagercoil block, southern India: Vestiges of paleoproterozoic arc and implications for columbia to gondwana. *Geosci. Front.* 12, 101126–126. doi:10.1016/j.gsf.2020.12.007

George, P. M., Sajeev, K., Santosh, M., and Zhai, M. (2019). Granulite-grade garnet pyroxenite from the Kolli-massif, southern India: Implications for Archean crustal evolution. *Lithos* 342, 499–512. doi:10.1016/j.lithos.2019.05.040

Green, E. C. R., White, R. W., Diener, J. F. A., Powell, R., Holland, T. J. B., and Palin, R. M. (2016). Activity-composition relations for the calculation of partial melting equilibria for metabasic rocks. *J. Metamorph. Geol.* 34, 845–869. doi:10.1111/jmg.12211

Hansen, E. C., and Harlov, D. E. (2007). Whole rock, phosphate, and silicate compositional trends across an amphibolite-to granulite-facies transition, Tamil Nadu, India. *J. Petrology* 86, 1641–1680. doi:10.1093/petrology/egm031

Harlov, D. E., and Hansen, E. C. (2005). Oxide and sulphide isograds along a late Archean, deep-crustal profile in Tamil Nadu, south India. *J. Metamorph. Geol.* 23, 241–259. doi:10.1111/j.1525-1314.2005.00574.x

Harlov, D. E., Wirth, R., and Forster, H. J. (2005). An experimental study of dissolution–reprecipitation in fluorapatite: fluid infiltration and the formation of monazite. *Contrib. Mineral. Pet.* 150, 268–286. doi:10.1007/s00410-005-0017-8

Holland, T. J. B., and Powell, R. A. (1991). Compensated-Redlich-Kwong (CORK) equation for volumes and fugacities of CO2 and H2O in the range 1 bar to 50 kbar and 100–1600 ◦C. *Contr. Mineral. Pet.* 109, 265–273. doi:10.1007/bf00306484

Holland, T. J. B., and Powell, R. (2003). Activity–composition relations for phases in petrological calculations: an asymmetric multicomponent formulation. *Contrib. Mineral.* . 145, 492–501. doi:10.1007/s00410-003-0464-z

Holland, T. J. B., and Powell, R. (1998). An internally-consistent thermodynamic dataset for phases of petrological interest. *J. Metamorph. Geol.* 16, 309–343. doi:10.1111/j.1525-1314.1998.00140.x

Holland, T. J. B., and Powell, R. (2011). An improved and extended internally consistent thermodynamic dataset for phases of petrological interest, involving a new equation of state for solids. *J. Metamorph. Geol.* 29, 333–383. doi:10.1111/j.1525-1314.2010.00923.x

Jayananda, M., Santosh, M., and Aadhiseshan, K. R. (2018). formation of archean (3600–2500 Ma) continental crust in the dharwar craton, southern India. *Earth. Sci. Rev.* 181, 12–42. doi:10.1016/j.earscirev.2018.03.013

Kwon, S., Samuel, V. O., Song, Y., Kim, S. W., Park, S.-I., Jang, Y., et al. (2020). Eclogite resembling metamorphic disequilibrium assemblage formed through fluid-induced metasomatic reactions. *Sci. Rep.* 10, 19869. doi:10.1038/s41598-020-76999-y

Manning, C. E. (2018). Fluids of the lower crust: Deep is different. *Annu. Rev. Earth Planet. Sci.* 46, 67–97. doi:10.1146/annurev-earth-060614-105224

Mathew, A., Anilkumar, Y., Santosh, M., Gao, P., Yang, C. X., Anoop, K. S., et al. (2022). Mafic-ultramafic suite from the karwar block, SW India: Implications for mesoarchean geodynamics. *Precambrian Res.* 372, 106601. doi:10.1016/j.precamres.2022.106601

McDonough, W. F., Sun, S., Ringwood, A. E., Jagoutz, E., and Hofmann, A. W. (1991). K, Rb and Cs in the Earth and Moon and the evolution of the Earth's mantle. *Ross. Taylor Symp. Vol. Geochim. Cosmochim. Acta* 56, 1001–1012. doi:10.1016/0016-7037(92)90043-I

Meissner, B., Deters, P., Srikantappa, C., and Kohler, H. (2002). Geochronological evolution of the Moyar, Bhavani and Palghat shear zones of southern India, implications for east Gondwana correlations. *Precambrian Res.* 114, 149–175. doi:10.1016/S0301-9268(01)00222-4

Noh, J., Kim, C., Samuel, V. O., Jang, Y., Park, S.-I., and Kwon, S. (2020). Fluid infiltration and mass transfer along a lamprophyre dyke–marble contact: An example from the south-western Korean Peninsula. *Minerals* 10, 828. doi:10.3390/min10090828

Palin, R. M., White, R. W., Green, E. C. R., Diener, J. F. A., Powell, R., and Holland, T. J. B. (2016). High-grade metamorph- ism and partial melting of basic and intermediate rocks. *J. Metamorph. Geol.* 34, 871–892. doi:10.1111/jmg.12212

Pan, D., and Galli, G. (2016). The fate of carbon dioxide in water-rich fluids under extreme conditions. *Sci. Adv.* 2, e1601278. doi:10.1126/sciadv.1601278

Pan, D., Spanu, L., Harrison, B., Sverjensky, D. A., and Galli, G. (2013). Dielectric properties of water under extreme conditions and transport of carbonates in the deep Earth. *Proc. Natl. Acad. Sci. U. S. A.* 110, 6646–6650. doi:10.1073/pnas.1221581110

Pan, Y., and Fleet, M. E. (2002). Compositions of the apatite-group minerals: Substitution mechanisms and controlling factors. *Rev. Mineral. Geochem.* 48, 13–49. doi:10.2138/rmg.2002.48.2

Peucat, J. J., Jayananda, M., Chardon, D., Capdevila, R., Fanning, M., Paquette, C., et al. (2013). The lower crust of the dharwar craton, southern India: Patchwork of archean granulitic domains. *Precambrian Res.* 227, 4–28. doi:10.1016/j.precamres.2012.06.009

Prowatke, S., and Klemme, S. (2006). Trace element partitioning between apatite and silicate melts. *Geochim. Cosmochim. Acta* 70, 4513–4527. doi:10.1016/j.gca.2006.06.162

Pyle, J. M., Spear, F. S., and Wark, D. A. (2002). "Electron micro probe analysis of REE in apatite, monazite and xenotime: Protocols and pitfalls," in *Phosphates—geochemical, geobiological, and materials importance*. Editors M. J. Kohn, J. Rakovan, and J. M. Hughes (USA: Mineralogic Society of America), 337–362.

Radhakrishna, B. P. (1989). Suspect tectono-stratigraphic terrain elements in the Indian sub-continent. *J. Geol. Soc. India* 34, 1–24.

Raith, M., Srikantappa, C., Köhler, H., and Buhl, D. (1999). The Nilgiri enderbites, south India: nature and age constraints on protolith formation, high-grade metamorphism and cooling history. *Precambrian Res.* 98, 129–150. doi:10.1016/S0301-9268(99)00045-5

Ratheesh-Kumar, R. T., Windley, B. F., Xiao, W. J., Jia, X. L., Mohantyi, D. P., and Zeba-Nezrin, F. K. (2020). Early growth of the Indian lithosphere: implications from the assembly of the dharwar craton and adjacent granulite blocks, southern India. *Precambrian Res.* 336, 105491–105528. doi:10.1016/j.precamres.2019.105491

Rebay, G., Powell, R., and Diener, J. F. A. (2010). Calculated phase equilibria for a MORB composition in a P–T range, 450–650°C and 18–28 kbar: The stability of eclogite. *J. Metamorph. Geol.* 28, 635–645. doi:10.1111/j.1525-1314.2010.00882.x

Samuel, V. O., Harlov, D. E., Kwon, S., and Sajeev, K. (2019). Silicate, oxide and sulphide trends in neo-archean rocks from the Nilgiri block, southern India: the role of fluids during high-grade metamorphism. *J. Petrology* 60, 1027–1062. doi:10.1093/petrology/egz023

Samuel, V. O., Kwon, S., Santosh, M., and Sajeev, K. (2018). Garnet pyroxenite from Nilgiri block, southern India: vestiges of a neoarchean volcanic arc. *Lithos* 310–311, 120–135. doi:10.1016/j.lithos.2018.04.009

Samuel, V. O., Sajeev, K., Hokada, T., Horie, K., and Itaya, T. (2015). Neoarchean arc magmatism followed by high-temperature, high-pressure metamorphism in the Nilgiri Block, southern India. *Tectonophysics* 662, 109–124. doi:10.1016/j.tecto.2015.06.035

Samuel, V. O., Santosh, M., Jang, Y., and Kwon, S. (2021). Acidic fluids in the Earth's lower crust. *Sci. Rep.* 11, 21146. doi:10.1038/s41598-021-00719-3

Samuel, V. O., Santosh, M., Liu, S., Wang, W., and Sajeev, K. (2014). Neoarchean continental growth through arc magmatism in the Nilgiri Block, southern India. *Precambrian Res.* 245, 146–173. doi:10.1016/j.precamres.2014.02.002

Samuel, V. O., Santosh, M., Yang, Q. Y., and Sajeev, K. (2016). Geochemistry and zircon geochronology of the Neoarchean volcano-sedimentary sequence along the northern margin of the Nilgiri Block, southern India. *Lithos* 263, 257–273. doi:10.1016/j.lithos.2016.01.027

Santosh, M. (1992). Carbonic fluids in granulites: cause or consequence? *J. Geol. Soc. India* 39, 375–399.

Santosh, M. (1986). Carbonic metamorphism of charnockites in the south western Indian shield: A fluid inclusion study. *Lithos* 19, 1–10. doi:10.1016/0024-4937(86)90011-3

Santosh, M., Harris, N. W., Jackson, D. H., and Mattey, D. P. (1990). Dehydration and incipient charnockite formation: a phase equilibria and fluid inclusion study from south India. *J. Geol.* 98, 915–926. doi:10.1086/629461

Santosh, M., Hu, C. N., He, X. F., Li, S. S., Tsunogae, T., Shaji, E., et al. (2017). Neoproterozoic arc magmatism in the southern madurai block, India: subduction, relamination, continental outbuilding, and the growth of gondwana. *Gondwana Res.* 45, 1–42. doi:10.1016/j.gr.2016.12.009

Santosh, M., Maruyama, S., and Sato, K. (2009). Anatomy of a cambrian suture in gond-wana: Pacific-type orogeny in southern India? *Gondwana Res.* 16, 321–341. doi:10.1016/j.gr.2008.12.012

Santosh, M., Shaji, E., Tsunogae, T., Ram-Mohan, M., Satyanarayanan, M., and Horie, K. (2013). Suprasubduction zone ophiolite from agali hill: Petrology, zircon SHRIMP U-Pb geochronology, geochemistry and implications for neoarchean plate tectonics in southern India. *Precambrian Res.* 231, 301–324. doi:10.1016/j.precamres.2013.04.003

Santosh, M. (2020). The southern granulite terrane: A synopsis. *Episodes* 43, 109–123. doi:10.18814/epiiugs/2020/020006

Santosh, M., Yang, Q. Y., Shaji, E., Tsunogae, T., Ram-Mohan, M., and Satyanarayanan, M. (2015). An exotic mesoarchean microcontinent: the Coorg block, southern India. *Gondwana Res.* 27, 165–195. doi:10.1016/j.gr.2013.10.005

Srikantappa, C., Raith, M., and Touret, J. L. R. (1992). Synmetamorphic high-density carbonic fluids in the lower crust: Evidence from the Nilgiri granulites, southern India. *J. Petrology* 4, 733–760. doi:10.1093/petrology/33.4.733

Stolte, N., and Pan, D. (2019). Large presence of carbonic acid in CO2-rich aqueous fluids under Earth's mantle conditions. *J. Phys. Chem. Lett.* 10, 5135–5141. doi:10.1021/acs.jpclett.9b01919

Thompson, A. B. (1992). Water in the Earth's upper mantle. *Nature* 358, 295–302. doi:10.1038/358295a0

Touret, J. L. R., and Hansteen, T. H. (1988). Geothermobarometry and fluid inclusions in a rock from the doddabetta charnockite complex. *South. India. Soc. Ital. Mineral.* . 43, 65–82.

Wang, J. Y., and Santosh, M. (2019). Eoarchean to Mesoarchean crustal evolution in the Dharwar craton, India: Evidence from detrital zircon U-Pb and Hf isotopes. *Gondwana Res.* 72, 1–14. doi:10.1016/j.gr.2019.02.006

Wang, J. Y., Santosh, M., Jayananda, M., and Aadhiseshan, K. R. (2020). Bimodal magmatism in the eastern dharwar craton, southern India: Implications for neoarchean crustal evolution. *Lithos* 354, 105336. doi:10.1016/j.lithos.2019.105336

White, R. W., Powell, R., and Clarke, G. L. (2002). The interpretation of reaction textures in Fe-rich metapelitic granulites of the musgrave block, central Australia: constraints from mineral equilibria calculations in the system K2O–FeO–MgO– Al2O3–SiO2–H2O–TiO2–Fe2O3. *J. Metamorph. Geol.* 20, 41–55. doi:10.1046/j.0263-4929.2001.00349.x

White, R. W., Powell, R., Holland, T. J. B., Johnson, T. E., and Green, E. C. R. (2014). New mineral activity-composition relations for thermodynamic calculations in metapelitic systems. *J. Metamorph. Geol.* 32, 261–286. doi:10.1111/jmg.12071

Yang, C. X., Santosh, M., Li, S. S., Shaji, E., and Kim, S. W. (2022). The paleoproterozoic magmatic arc of trivandrum block, southern India: From columbia to gondwana. *Precambrian Res.* 372, 106612. doi:10.1016/j.precamres.2022.106612

Yang, C. X., Santosh, M., Tsunogae, T., Shaji, E., Gao, P., and Kwon, S. (2021). Global type area charnockites in southern India revisited: Implications for Earth's oldest supercontinent. *Gondwana Res.* 94, 106–132. doi:10.1016/j.gr.2021.03.003

Yu, B., Santosh, M., Wang, M. X., and Yang, C. X. (2022). Paleoproterozoic emplacement and Cambrian ultrahigh-temperature metamorphism of a layered magmatic intrusion from the Central Madurai Block, southern India: From Columbia to Gondwana. *Geosci. Front.* 13, 101260. doi:10.1016/j.gsf.2021.101260